UNIVERSITY OF TWENTE.

Faculty of Electrical Engineering,
Mathematics & Computer Science

Characterizing Large-Form-Factor Devices in a Reverberation Chamber

Stefan van de Beek
M.Sc. Thesis
August 2012

Graduation committee:
Prof. dr. ir. F.B.J. Leferink
Dr. ir. M.J. Bentum
Dr. ir. G. Heijenk
Dr. C.L. Holloway
Dr. K.A. Remley

Telecommunication Engineering Group
Faculty of Electrical Engineering,
Mathematics and Computer Science
University of Twente
P.O. Box 217
7500 AE Enschede
The Netherlands

Summary

With new technologies such as machine-to-machine communications there is a growing need to test large-form-factor devices in reverberation chambers. The performance of the reverberation chamber can be affected by the physical characteristics of these devices. In this report it is discussed how the spatial uniformity of the received stirred power and the received total power (stirred + unstirred power) are affected by a large object. A distinction is made between reflecting and absorbing objects. The chamber was loaded by stacking metallic boxes (cardboard boxes wrapped in aluminium foil), or by stacking RF absorbers. The metallic boxes slightly load the chamber. Measurements show that this is caused by the cardboard being lossy. The absorbers significantly load the chamber.

It is shown that large metallic objects cause minimal degradation in the spatial uniformity. Absorbing objects can cause substantial degradation in the spatial uniformity, motivating the need for testing guidelines for these objects. The spatial uniformity with respect to the total received power degrades because the unstirred energy becomes more dominant for a loaded chamber. The unstirred components are the energy that is coupled from the transmitter to the receiver without interacting with the paddle. The stirred component is the energy that interacts with the paddle.

If the unstirred components are removed, the spatial uniformity still degrades with increasing numbers of absorbers. A reason for this degradation is found in the proximity effect. The proximity effect is explained by the fact that an absorber in close proximity of an antenna appears to be larger, and is for this reason more likely to occupy a larger amount of the antenna pattern. The absorber does not reflect electromagnetic waves, so an antenna in close proximity of an absorber will receive less power.

In future work, the effect of absorbers on the spatial uniformity of the stirred power will be further investigated. It is proposed to study the spatial uniformity in the chamber when it is corrected for the proximity effect.

Contents

Summary **iii**

1 Introduction **1**

2 Theory of the reverberation chamber **5**

2.1 Electromagnetic Environment 5
2.2 Spatial Uniformity 6
2.3 Quality factor of the chamber 8

3 Measurement campaign **11**

3.1 Experimental setup 11
3.2 Scattering parameters 13
3.3 Coefficient of variation 14
3.4 Quality factor and decay time 15

4 Reverberation chamber Q and PDP **17**

4.1 Power delay profile 17
4.2 Quality factor 18

5 Spatial Uniformity **23**

5.1 Measurements in the reverberation chamber and uncertainties 23
5.2 K-factor 25
5.3 Coefficient of variation 26

6 Proximity Effect **33**

6.1 Definition of the proximity effect 33
6.2 Validation of the proximity effect 33

7 Conclusion and Recommendations **37**

References **38**

Chapter 1

Introduction

New technologies such as machine-to-machine (M2M) communications are becoming commonplace, and these M2M devices need to be characterized and tested for radiated emissions and radiated susceptibility. Some of the M2M devices can be large-form-factor devices. While small devices can be tested with current methods in the anechoic chamber, the use of anechoic chambers may not be practical for large devices. Reverberation chambers could be useful for physically large devices, providing a reliable and repeatable test environment.

In recent years reverberation chambers have been used more and more as a facility for characterizing and testing devices, see [1, 2] for a list of applications. A common reverberation chamber consists of a closed cavity with conducting walls and an arbitrarily shaped metallic rotating paddle (stirrer). A reverberation chamber has a high quality factor (Q) which allows a high field to be built up inside the chamber. When a driven antenna is located in the chamber it will excite a large number of electromagnetic (EM) modes that have resonances near the frequency of excitation. The paddle continuously alters the boundary conditions of the EM-fields inside the chamber. Without the rotating paddle the field strength is very strongly dependent on the location in the chamber, i.e. there are locations with very high field values and very low field values. By moving the stirrer the energy in the chamber is redistributed, and all locations in the chamber will experience the same maxima and minima fields. There are many other types of reverberation chambers that rely on different ways of stirring the field, e.g., position stirring or frequency stirring. The same theory applies in reverberation chambers regardless of the stirring method. If the chamber is well stirred and there exists a highly overmoded condition the field is proven to be; (1) randomnly polarised, i.e. the phase between all waves is random, (2) spatially uniform, i.e. the energy density in the chamber is uniform everywhere, and (3) isotropic, i.e. the energy flow is in all directions the same [3, 4].

The performance of the reverberation chamber can be affected by the physical characteristics of the device-under-test (DUT). A DUT can load the chamber and this loading will alter characteristics of the chamber [5]. In [6,7] it was shown that loading a chamber reduces the spatial uniformity. In [6] equations are derived for maximum loading expressed in a threshold quality factor Q_{thr}. For an effective reverberation chamber, the Q should exceed this threshold value. However, in [6] the question remains on how to relate the spatial uniformity to the Q of the chamber.

Often an M2M device is mainly metallic and for this reason will not significantly increase the loss in the chamber, i.e., the chamber will not be excessively loaded. However, physically large M2M devices will have significant dimensions compared to the dimensions of the chamber and that could affect the performance of the chamber. The effect of a large object that occupies a significant amount of the working volume in the reverberation chamber is one key aspect of this thesis. A second aspect focuses on M2M devices that are constructed out of lossy materials. Such devices will load the chamber.

One important characteristic of a wireless device such as an M2M device is its total radiated power (TRP). In [8] a method is described to measure the TRP using a reverberation chamber. To ensure a low uncertainty in the TRP measurement, it is important to have a spatially uniform field distribution throughout the chamber, i.e., the energy density in the chamber should be as uniform as possible. This will ensure that the measurement results are independent of the exact location (within the working volume) of the receiving antenna and of the DUT. The spatial uniformity in the chamber can be characterized by calculating the standard deviation of the mean field for measurements made throughout the chamber. A low standard deviation of the mean field indicates that; (1) there are a sufficient number of modes in the chamber, (2) the paddle is large enough to interact with the modes, and (3) the set of independent data points is sufficiently high for a given paddle movement.

For wireless communications, an important parameter of the multipath EM-environment is the Rician K-factor. The K-factor describes the power ratio between the direct path component and the scattered multipath components [9,10]. The reverberation chamber may be used as a test facility to simulate this parameter [1,11]. In these papers it is shown that the K-factor is affected by loading of the chamber.

Another imporant parameter for an multipath EM-environment is the power delay profile (PDP) and the accompanying root mean square (RMS) delay spread. The PDP gives the power of a signal received through a multipath channel as a function of propagation delay relative to the delay of the shortest path [9,10]. The PDP of a typical multipath environment can also be simulated in a reverberation chamber. The PDP and RMS delay spread depend on the quality factor of the chamber [2,12].

In this thesis, we characterize the effect of a large device on the spatial uniformity, K-factor and Q in the chamber. We will show equations that relate Q to the spatial uniformity. The field distribution is measured and compared at several different points in the chamber. It will be shown how the K-factor in the reverberation chamber is related to the spatial uniformity. The uniformity of the field in close proximity to a large object is also studied. A distinction is made between the effects of an electromagnetically reflecting object and an absorbing object in the chamber. The aim of this research is to better understand the reverberation chamber and to help develop guidelines for characterizing and testing large-form-factor wireless devices in reverberation chambers. The research question in this this report is: "How does a large-form-factor device affect the characteristics of a reverberation chamber?".

This report is structured as follows: in Chapter 2, the theory of the electromagnetic environment in a reverberation chamber is briefly summarized, and the concept of spatial uniformity is explained. In Chapter 3, the measurement campaign that is used to experimentally study the effect of a large-form-factor device on the reverberation chamber performance is explained. In Chapter 4 and Chapter 5, the results of the chamber Q and spatial uniformity are presented and discussed. Next, in Chapter 6, the effect of an antenna in close proximity to an absorber is studied. Finally, in Chapter 7, conclusions are drawn and recommendations for future work are made.

Chapter 2

Theory of the reverberation chamber

In this section, the underlying theory in reverberation chambers with respect to the K-factor, spatial field uniformity and the quality factor is explained. First, the electromagnetic environment in a reverberation chamber is briefly revisited. A statistical model is developed that describes the stochastic nature of the electromagnetic field. Second, the concept of spatial uniformity in a reverberation chamber is explained. At last, the Q of the chamber is explained and the relationship between Q and the K-factor.

2.1 Electromagnetic Environment

At every point in the reverberation chamber, the electromagnetic field can be described by the vector sum of three rectangular field components. Each electric-field component can be described by the in-phase and quadrature component. This results in six parameters that fully describe the electric field.

$$\begin{aligned} E_x &= E_{xr} + iE_{xi}, \quad E_y = E_{yr} + iE_{yi} \\ E_z &= E_{zr} + iE_{zi}. \end{aligned} \tag{2.1}$$

Here E_x, E_y, and E_z are the rectangular electric-field components in terms of their real and imaginary parts. In a well-operating reverberation chamber, all six components are Gaussian distributed with zero-mean and identical variances. This will result in a chi-distribution with two degrees of freedom for the magnitude of any rectangular field component [1, 13–15]. This is equivalent to the Rayleigh distribution, which is described by

$$f(|E_x|) = \frac{|E_x|}{\sigma^2} \exp\left[-\frac{|E_x|^2}{2\sigma^2}\right] U(|E_x|), \tag{2.2}$$

where U is the unit step function, $|E_x|$ is the magnitude of the x component of the electric field, and σ^2 is the variance of the real and imaginary parts. This is similar for the other field components. In [1] σ^2 is defined as

$$\sigma^2 = \frac{\eta\lambda Q P_t}{12\pi V}, \tag{2.3}$$

where η is the free-space impedance, λ is the wavelength in meters, Q is the quality factor of the chamber (will be explained later on in this chapter), P_t the transmitted power in watts, and V the volume of the chamber in m^3.

The Rayleigh distribution is valid in a well-performing reverberation chamber with no unstirred field components. The unstirred components consists of the energy that is coupled from the transmitter to the receiver without interacting with the paddle. A special case of the unstirred energy is the direct (line-of-sight) component. The stirred components consists of the energy that interacts with the paddle. The unstirred components are generally considered as a deterministic component that is superimposed on the stochastic electromagnetic field [16]. For this reason the mean value of the real and imaginary parts in (2.1) may not be zero, but the variance remains the same. As explained in [1,16] the distribution of the magnitude of a rectangular field component is in the presence of unstirred energy given by

$$\begin{aligned} f(|E_x|) &= \tfrac{|E_x|}{\sigma^2} I_0\left(\tfrac{|E_x||E_{dx}|}{\sigma^2}\right) \\ &\quad \times \exp\left[-\tfrac{|E_x|^2+|E_{dx}|^2}{2\sigma^2}\right] U(|E_x|). \end{aligned} \tag{2.4}$$

Here I_0 is the modified Bessel function of zeroth order, and E_{dx} is the unstirred component. The distribution in (2.4) is called the Rician distribution.

A Rician distribution is characterized by the Rician K-factor, which is defined as the ratio of the signal power in the unstirred components over the stirred power. In a reverberation chamber, the scattered power is represented by $2\sigma^2$ [1], and the unstirred power is $|E_{dx}|^2$

$$K = \frac{\text{unstirred components}}{\text{scattered components}} = \frac{|E_{dx}|^2}{2\sigma^2}. \tag{2.5}$$

For $K = 0$ equation (2.4) reduces to a Rayleigh distribution. Typically in reverberation chambers the K-factor is very low, but not zero. The K-factor is an important parameter to define the electromagnetic environment in a reverberation chamber.

2.2 Spatial Uniformity

In [8], a procedure is described to measure the TRP of a DUT. The uncertainties associated with a TRP measurement are explained in [17]. As mentioned in the introduction, it is important to have a spatially uniform field inside the reverberation chamber to achieve a low uncertainty in the TRP measurement. Another important condition, as is explained in [17], is to minimize the unstirred power, for example, by pointing the the measurement antenna at a stirrer.

Under the assumption that there are no unstirred components, the spatial field uniformity in the chamber can be theoretically calculated. In the absence of unstirred components, the electric field components in a reverberation chamber are Rayleigh distributed as in (2.2). The power received by an antenna is then proportional to the square of the E-field component and has an exponential distribution [18];

$$f(|E_x|^2) = \frac{1}{2\sigma^2} \exp\left[-\frac{|E_x|^2}{2\sigma^2}\right]. \tag{2.6}$$

In an exponential distribution, the mean is equal to the variance. So, the mean received power μ_p and the standard deviation σ_p of the received power in a reverberation chamber are equal and are given by $2\sigma^2$.

If at several positions throughout the chamber N samples of the received power are taken the sample mean at these locations can be calculated from these N samples. An estimate of μ_p would consist of an average of the sample mean powers received at the several locations. From the Central Limit Theorem it is known that if the samples are independent the distribution of this average tends to be normal. In [19] it is explained that if the N samples are uncorrelated this normal distribution will have the mean in (2.6), and the standard deviation σ_s in the estimate of the mean power will be given by

$$\sigma_s = \frac{\sigma_p^2}{\sqrt{N}} = \frac{2\sigma^2}{\sqrt{N}}. \tag{2.7}$$

In this thesis we compare the spatial field uniformity for different loading configurations. Different loading configurations will cause a change in the received mean power $2\sigma^2$ [5,6]. To compare values of standard deviations for different loading configurations it should be normalized. The normalized measure is called the coefficient of variation C_v and is given by

$$C_v = \frac{\sigma_s}{2\sigma^2} = \frac{1}{\sqrt{N}}. \tag{2.8}$$

From this equation, it can be concluded that the spatial uniformity of the scattered power from a Rayleigh distributed field only depends on the number of independent samples taken in the reverberation chamber.

Obviously, the unstirred components in the reverberation chamber are dependent on location. So when a significant number of unstirred components are present, the spatial uniformity will decrease. This can be well characterized by the Rician K-factor (2.5). When the chamber is loaded, the Q will decrease, and from (2.3), it can be seen that the stirred power will decrease. As a result the K-factor will increase because the unstirred components are more dominant, and the spatial field uniformity of the total received power (stirred + unstirred) will degrade.

2.3 Quality factor of the chamber

One of the most common figure of merits when discussing reverberation chambers is the Q of the chamber. The quality factor is defined by

$$Q = \frac{\omega U}{P_d}, \tag{2.9}$$

where ω is the angular frequency, U is the energy stored in the cavity and P_d is the power dissipated. For steady state conditions the dissipated power P_d equals the transmitted power P_t in a reverberation chamber [18]. In [18] it is explained that there are four types of loss that contribute to P_d. That is; (1) loss due to power dissipated in the walls, (2) loss due to power absorbing objects in the chamber, (3) the leakage through apertures, and (4) loss due to the power dissipated in the loads of receiving antennas. For an unloaded reverberation chamber the wall losses are usually dominant.

The mean-square electric field E_0^2 in a reverberation chamber is represented by

$$E_0^2 = \frac{QP_t}{\omega \epsilon V}, \tag{2.10}$$

where ϵ is the electrical permittivity of the free space in the reverberation chamber and V is the volume of the chamber. From [18] we know that

$$\frac{E_0^2}{6} = \sigma^2. \tag{2.11}$$

Since the stirred power is represented by $2\sigma^2$ we can conclude that the stirred power is directly proportional to E_0 and thus to Q. To create a Rayleigh distribution the K-factor (2.5) needs to approach zero, so the Q needs to be very high.

However, as explained in [4, 6] an infinite Q will exhibit a line spectrum in the measured field, causing the chamber not to work continuously across the frequency. The bandwidth of the chamber mode is proportonial to the Q by

$$\Delta f = \frac{f_c}{Q}, \tag{2.12}$$

where f_c is the center frequency, and Δf is the mode bandwidth [12, 20]. Thus by lowering the Q the mode overlap will increase and this will smooth the EM field uniformity [4].

It has already been shown in [6, 7] that a too low Q will degrade the spatial uniformity. Holloway *et al.* derived a threshold quality factor Q_{thr},

$$Q_{thr} = \left(\frac{4}{3}\pi\right)^{2/3} \frac{3V^{1/3}}{2\lambda Q}. \tag{2.13}$$

The requirement for an effective reverberation chamber is $Q >> Q_{thr}$. The fundament of this derivation is that the stirred power must be much higher than the unstirred power. If the Q gets too low, the unstirred components will become more dominant. This will lead to an increase in the K-factor (2.5). As a result the spatial uniformity will decrease, since the unstirred components are inherently spatially dependent.

Another disadvantageous of a low Q is explained in [4,21]. The number of independent samples for one stirrer revolution decreases when the chamber Q decreases. With a lower Q the paddle is less efficient in stirring the EM-fields.

In the next chapter the measurement campaign will be presented that was performed to measure the Q, K-factor and spatial uniformity in the reverberation chamber.

Chapter 3

Measurement campaign

3.1 Experimental setup

Measurements were made in the NIST reverberation chamber with dimensions 4.6 m x 3.1 m x 2.8 m. A horn antenna and twelve NIST-fabricated monopoles were placed in various locations throughout the chamber, see Fig. 3.1. The monopoles were placed randomly throughout the chamber with different polarizations and heights.

The monopoles were tuned to a frequency of 1.9 GHz and mounted on groundplanes with dimensions 20 cm x 20 cm. The horn antenna is a dual-ridge horn antenna and the aperture dimension is 13.5 cm x 22.5 cm. In Fig. 3.2 the horn antenna and a monopole is depicted. The free-space reflection coefficients of all 12 monopoles and the horn antenna are measured in the reverberation chamber. Results are plotted in Fig. 3.3. In the next section it will be explained how the free-space reflection coefficients of

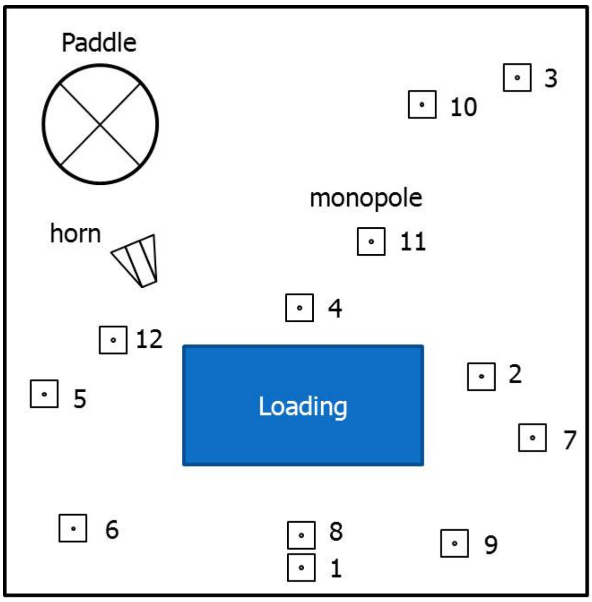

Figure 3.1: Top view of setup in the reverberation chamber.

(a)

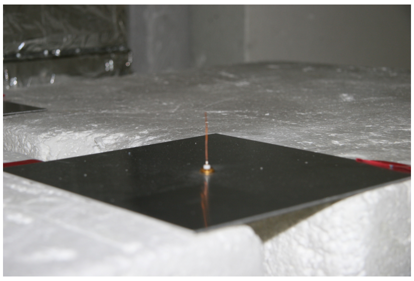

(b)

Figure 3.2: The antennas used in this study: (a) dual-ridge horn antenna and (b) monopole on a groundplane.

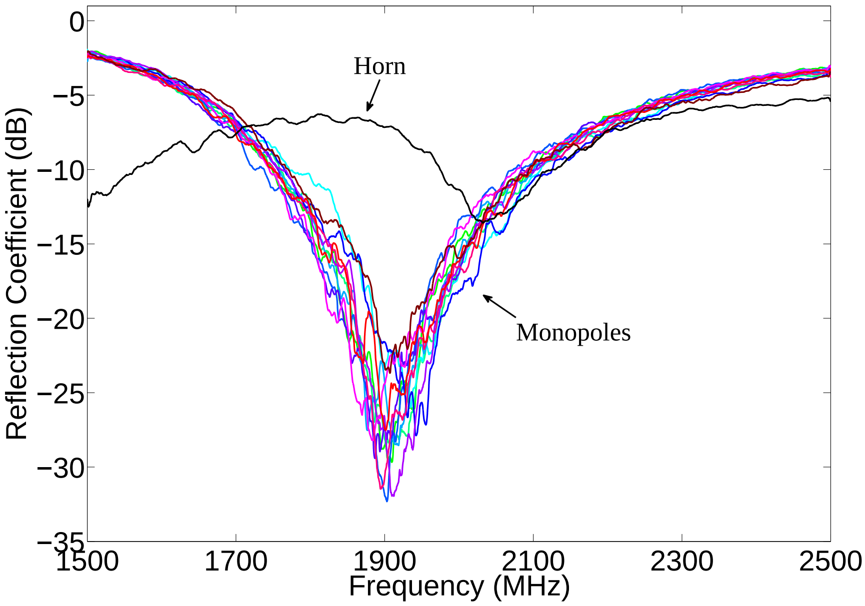

Figure 3.3: Reflection coefficients of the individual monopoles and the horn antenna as a function of frequency. The data is smoothed over 18.75 MHz.

antennas can be measured in a reverberation chamber.

Fig. 3.1 also designates the location of the test loading placed near the middle of the chamber. The loading in the chamber was obtained by stacking metallic boxes with dimensions 0.61 m x 0.41 m x 0.32 m (Fig. 3.4(a)) or by stacking radio-frequency (RF) absorbers (Fig. 3.4(b)). The geometry of an absorber is pyramidal. The length, width, and height are 0.6 m. Two stacked absorbers have a height of 0.7 m. The metallic boxes were made by wrapping cardboard boxes in aluminium foil.

The chamber was incrementally loaded by increasing the number of boxes or absorbers. The number of boxes in the chamber was incremented by 2 from 0 to 12. The number of absorbers in the chamber was incremented by 1 from 0 to 6. For

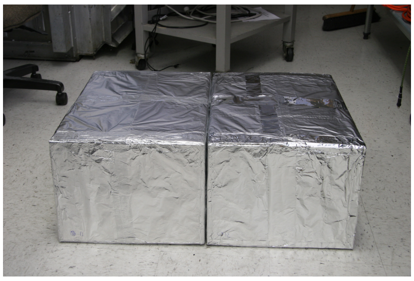

(a)

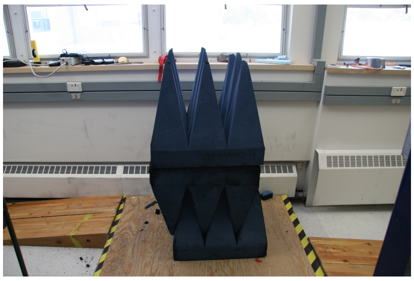

(b)

Figure 3.4: Loading for the reverberation chamber: (a) Metallic boxes or (b) RF absorbers.

every loading configuration the scattering parameter S_{21} between the horn and each single monopole was measured over 72 stirrer positions with a vector network analyzer (VNA). The stirrer was rotated 5 degrees from position to postion, so 72 samples were collected over a full 360° revolution of the stirrer. For every stirrer position 16000 frequency points from 1.5 GHz to 2.5 GHz were measured. A picture of the setup with 12 boxes in the chamber can be seen in Fig. 3.5.

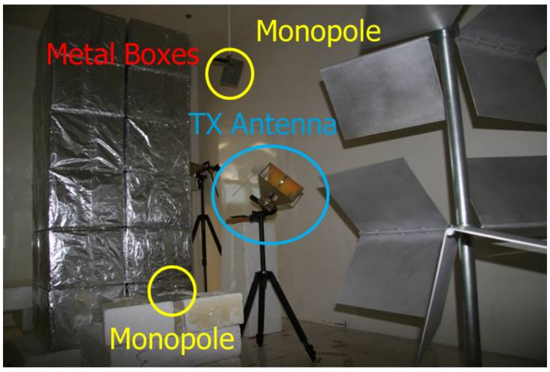

Figure 3.5: Chamber configuration for testing with 12 metallic boxes. The transmitting antenna was aimed at the stirrer, and monopoles were placed randomly throughout the chamber.

3.2 Scattering parameters

With use of the VNA the complex scattering parameters (S-parameters) between the horn and monopoles were measured. In [16] it has been shown that the statistics of S_{21} are similar to the statistics of the field components in the reverberation chamber. Essentially, S_{21} is the transfer function of the radio-propagation environment [1]. In [22–24] it is explained how the received power can be corrected for antenna mismatch.

As such, the total received power (stirred + unstirred power) can be described by:

$$\langle |S_{21}|^2 \rangle_{cor} = \frac{\langle |S_{21}|^2 \rangle}{(1 - |\langle S_{11} \rangle|^2)(1 - |\langle S_{22} \rangle|^2)}, \tag{3.1}$$

where the ensemble average is taken over all paddle positions. The term $\langle |S_{21}|^2 \rangle_{cor}$ represents the stirred + the unstirred power. The terms $|\langle S_{11} \rangle|^2$ and $|\langle S_{22} \rangle|^2$ are the free-space reflection coefficients of the horn antenna and the monopoles as is explained in [20,25]. This method has also been used to calculate and plot the free-space reflection coefficients in Fig. 3.3.

In [1] it was described how the stirred component can be calculated from the scattering parameters. The unstirred components are related to the mean value of S_{21}, and can be simply subtracted from S_{21}. As such, the stirred power can be described by

$$2\sigma^2 = \frac{\langle |S_{21} - \langle S_{21} \rangle|^2 \rangle}{(1 - |\langle S_{11} \rangle|^2)(1 - |\langle S_{22} \rangle|^2)}, \tag{3.2}$$

The power in the unstirred components, if not corrected for antenna mismatch, is represented by $|\langle S_{21} \rangle|^2$. So the K-factor can be calculated from S_{21} by [1] as:

$$K = \frac{|\langle S_{21} \rangle|^2}{\langle |S_{21} - \langle S_{21} \rangle|^2 \rangle}. \tag{3.3}$$

In this equation the mismatch correction for the unstirred power and the stirred power cancel each other out.

For every monopole the total received power, stirred received power, and K-factor were calculated.

3.3 Coefficient of variation

For every monopole we can calculate the sample mean over the 72 paddle positions. So for every frequency point we got twelve values of received power, i.e., the power received at the twelve locations by the monopoles. The mean power in the reverberation chamber μ_p was determined by averaging over these twelve values. The coefficient of variation C_v was determined by calculating the standard deviation σ_s over the received power at twelve locations and normalizing this standard deviation by μ_p.

$$C_v = \frac{\sigma_s}{\mu_p} \tag{3.4}$$

For a well-performing reverberation chamber, the C_v determined from the measurements should be equal to the C_v derived in the previous chapter, that is, equation (2.8).

The C_v was calculated for the total received power and the stirred received power.

3.4 Quality factor and decay time

The Q was determined from measuremens by making use of the fact that the losses, and so the Q, in the chamber are related to the decay time [18].

$$Q = \omega\tau_{RC} \tag{3.5}$$

In this equation τ_{RC} represents the decay time of the chamber in seconds, and ω is the angular frequency.

The τ_{RC} was determined from the PDP of the multipath channel in the reverberation chamber [2,26]. The PDP is the received power as a function of excess delay. The excess delay is defined as the propagation delay relative to the delay of the shortest path. Since the impulse respons $h(t)$ characterizes the multipath channel the PDP can be calculated from $h(t)$ of the chamber [10]. The PDP in the chamber is given by [2]

$$\mathrm{PDP}(t) = \langle |h(t,n)|^2 \rangle, \tag{3.6}$$

where the ensemble average is taken over the stirrer position n, and $h(t,n)$ is the impulse response of the chamber for the nth stirrer position. The impulse response $h(t,n)$ is given by

$$h(t,n) = \mathrm{IFT}[S_{21_n}(f)] \tag{3.7}$$

If the early time behavior of the reverberation chamber is neglected the PDP can be approximated by [26]

$$\mathrm{PDP}(t) = \langle |h(t,n)|^2 \rangle = P_o \, e^{-t/\tau_{RC}}. \tag{3.8}$$

In [26] it is shown that if the early time behavior is neglected the RMS delay spread is equal to τ_{RC}. The decay time τ_{RC}, or RMS delay spread, can now be determined by recognizing that the slope of $\ln[\mathrm{PDP}(t)]$ will be equal to $1/\tau_{RC}$.

Chapter 4

Reverberation chamber Q and PDP

In this chapter the PDP and Q for all the different loading configurations will be presented.

4.1 Power delay profile

The PDP was calculated using the measured S_{21} values over the band of frequencies from 1.5 GHz to 2.5 GHz. In Fig. 4.1 the PDP results are shown for all loading configurations. As can be seen the reflections damp out faster when the chamber gets loaded. The effect of the absorbers is much larger than the effect of the metallic boxes. The RMS delay spread for the loading configurations are shown in Table 4.1. These values show the decrease in decay time with increasing loading.

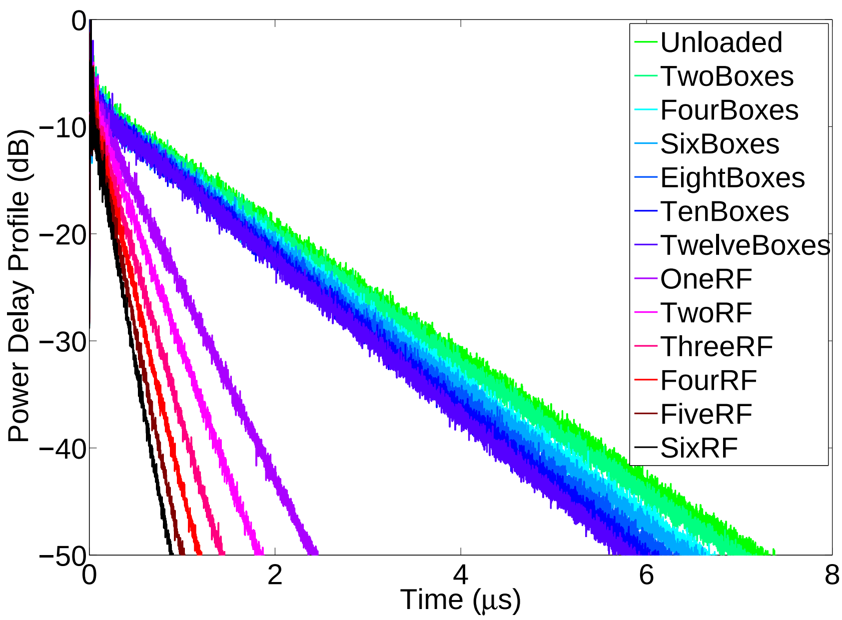

Figure 4.1: PDP for all loading configurations.

Table 4.1: RMS delay spread for all different loading configurations

Loading Configuration	RMS delay spread (ns)
Unloaded	733
Two boxes	715
Four boxes	684
Six boxes	666
Eight boxes	642
Ten boxes	620
Twelve boxes	603
One absorber	246
Two absorbers	187
Three absorbers	146
Four absorbers	122
Five absorbers	104
Six absorbers	93

4.2 Quality factor

The Q was determined determined every 100 MHz from 1600 MHz to 2400 MHz. The PDP and τ_{RC} were determined over a bandwidth of 200 MHz. In Fig. 4.2 the Q is plotted as a function of frequency for various loading configurations. The Q_{thr} (2.13) is also shown in this graph. It can be seen that the metallic boxes hardly affect the Q. The absorbers significantly load the chamber and the Q drops. The Q of the unloaded chamber is approximately a factor 100 higher than Q_{thr}, whereas the chamber with six absorbers is approximately a factor 10 higher. So even though the Q approaches the threshold, it is still well above Q_{thr}.

The effect of the metallic boxes can be seen better in Fig. 4.3, where the Q is plotted on a linear scale. In this figure the Q for various loading configurations with boxes is plotted and, for comparison, the Q for the one absorber configuration is plotted as well. It can be seen that the boxes slightly load the chamber.

The effect of metallic boxes on the Q was studied in more detail. As explained in [18] the reverberation chamber Q in case of dominant wall losses can be described as

$$Q = \frac{3V}{2\mu_r \delta A}. \tag{4.1}$$

In this equation V represents the volume of the reverberation chamber, μ_r is the relative permeability of the wall, $\delta = \sqrt{2/\omega\mu_w\sigma_w}$ is the skindepth, μ_w is the wall permeability, σ_w is the wall conductivity, and A is the wall surface area.

After placing metallic boxes in the chamber it was thought that the chamber was loaded by an increase of the wall losses. The decrease in volume is not significant, since 12 boxes occupy ony 2 percent of the total volume of the chamber. This means that if we would hang aluminium sheets in the chamber with the same surface area corresponding to the number of boxes the loading would be the same.

This hypothesis was tested by hanging aluminium sheets in the chamber corre-

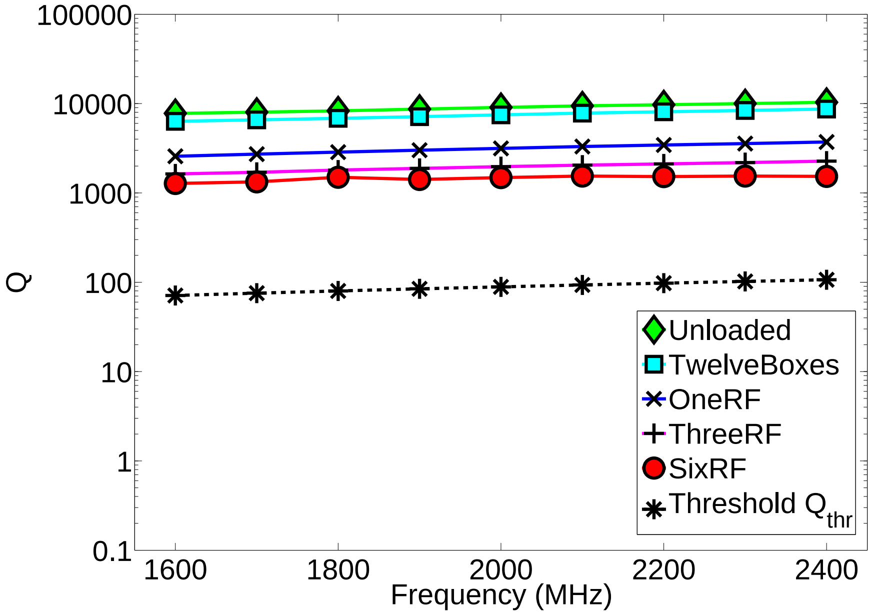

Figure 4.2: The quality factor Q on a logaritmic scale as a function of frequency. The different curves represent different loading configurations.

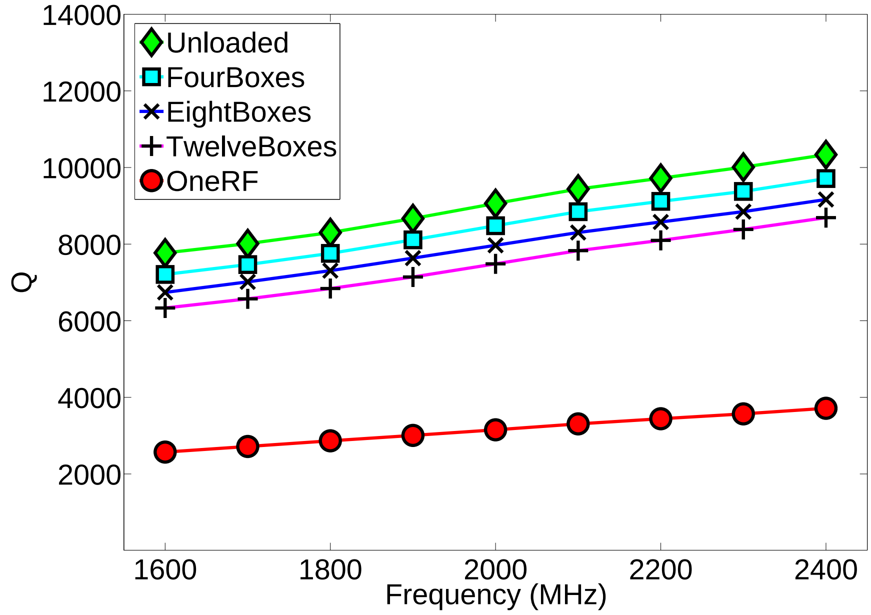

Figure 4.3: The quality factor Q on a linear scale as a function of frequency. The different curves represent different loading configurations.

sponding to 4 boxes, 8 boxes, and twelve boxes (Fig. 4.4). The Q for these loading configurations was measured and in Fig. 4.5 it is compared to the unloaded chamber and the chamber loaded by four boxes. As can be seen the sheets hardly load the

Figure 4.4: Aluminium sheets hang in the reverberation chamber.

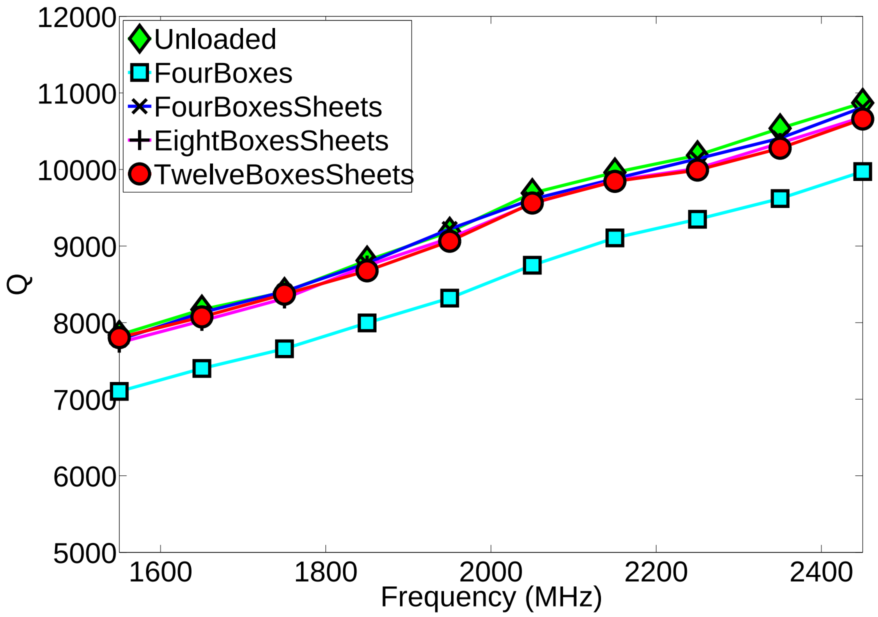

Figure 4.5: The Q as a function of frequency. The different curves are for the different loading configurations.

chamber and the effect on the Q can be neglected.

These results suggested that the cardboard boxes loaded the chamber. Apparently energy is coupled into the boxes and the cardboard boxes are lossy. This was shown more clearly by additional measurements. We measured the Q when the chamber was loaded by cardboard boxes without foil (Fig. 4.6(a)), cardboard boxes wrapped in foil (Fig. 4.6(b)), and cardboard boxes wrapped in foil with the seams closed by copper tape (Fig. 4.6(c)).

Results of these loading configurations together with the unloaded chamber are shown in Fig. 4.7. It can been that the bare cardboard boxes load the chamber, so it is concluded that the cardboard is lossy. When the boxes are wrapped in foil, the lossy material is partly shielded from the reverberation chamber. For this reason the Q is higher when the boxes are wrapped in foil. When we increase the shielding between the cardboard boxes and the chamber by closing the seams of the foil with copper tape the Q increases even higher.

These results show that the loading of the chamber with the metallic boxes is caused by the cardboard being lossy. Energy is coupled into the boxes and is absorber by the cardboard.

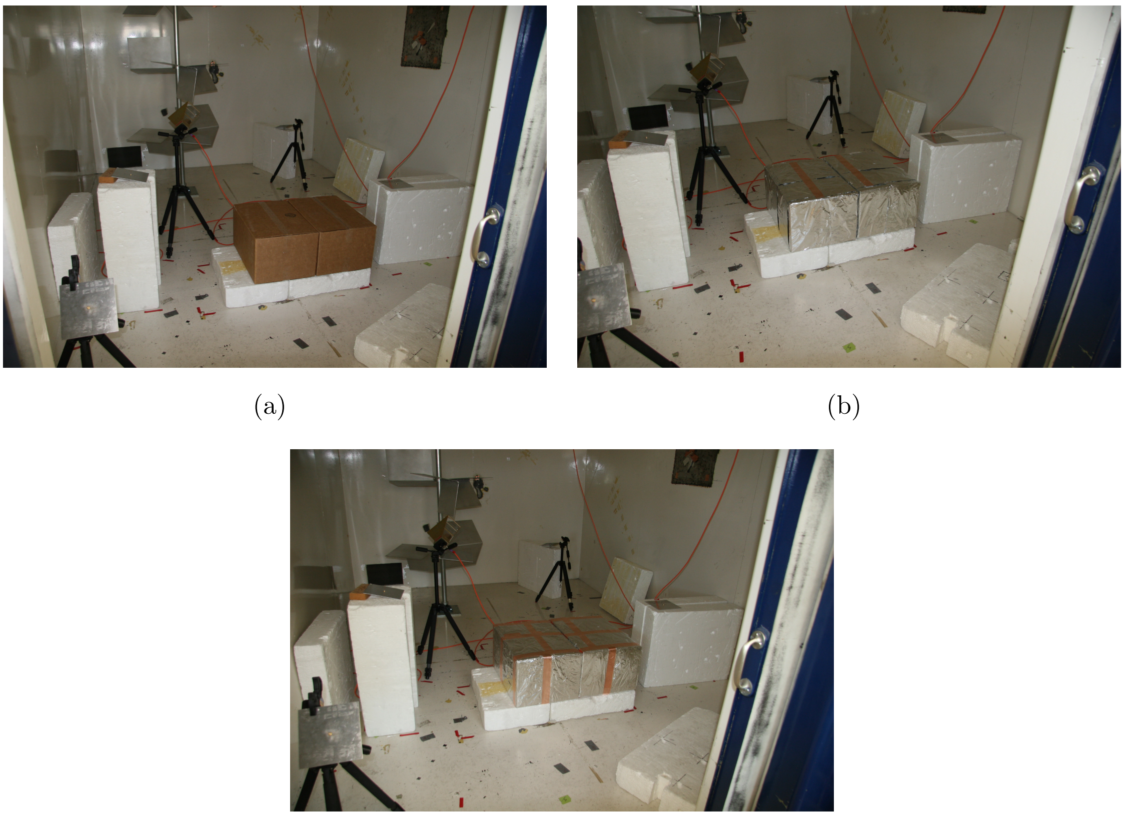

(a) (b) (c)

Figure 4.6: Different loading configurations.

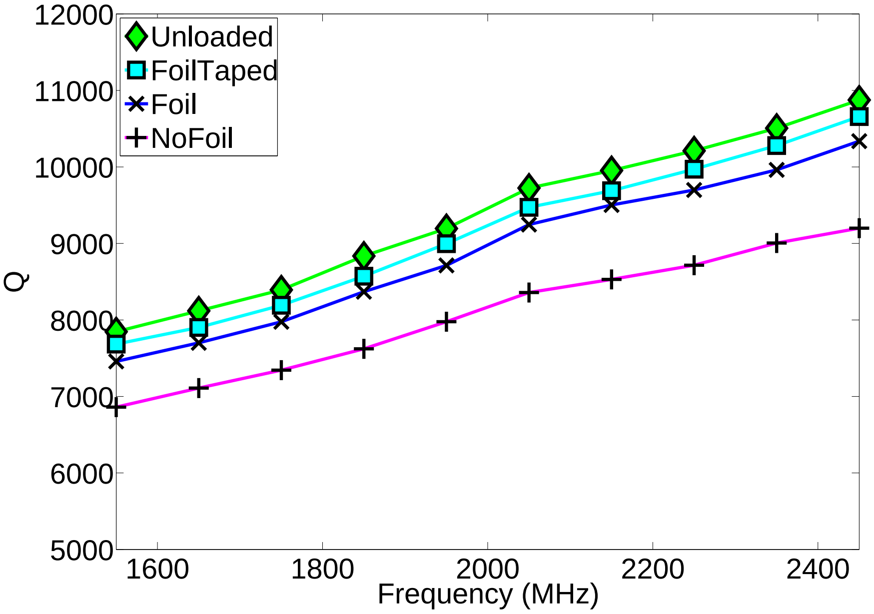

Figure 4.7: The Q as a function of frequency for the different loading configurations shown in Fig. 4.6.

Chapter 5

Spatial Uniformity

In this chapter the spatial uniformity for every loading configuration is studied. In the first section the results of the measurements of the total power and stirred power in the reverberation chamber are presented. Next, we look at the K-factor in the chamber. In the last section the spatial uniformity will be quantified by the coefficient of variation C_v.

5.1 Measurements in the reverberation chamber and uncertainties

In Fig. 5.1, we plot the total power (3.1) received by a monopole for various loading configurations as function of frequency. The received power is corrected for the mismatch of the antennas. The data are smoothed over 18.75 MHz to show the difference between various loading configurations more clearly. As can be seen, the received power decreases slightly as the number of boxes increases from unloaded to twelve metal boxes. The received power decreases rapidly when absorbers are put in the chamber. For the loading configurations with absorbers, we also see that the variability in the curve increases. This is due to the fact that the stirred energy decreases when the chamber is loaded, as can be seen from (2.3). The unstirred energy also drops if absorbers are placed in the chamber, but it is less affected by the absorbers than the stirred power. As a result, the unstirred components are more dominant. At a fixed location the unstirred components will be frequency dependent. In Fig. 5.2 the stirred power received by a is plotted as a function of frequency. The stirred power was calculated by (3.2). As expected, the variability of the individual curves is much less compared to the curves in Fig. 5.1.

The sources of uncertainties that are associated with measurements in the NIST reverberation chamber are extensively explained in [22]. In our case, we looked at the measurement system reproducibility, and the VNA drift. The measurement system

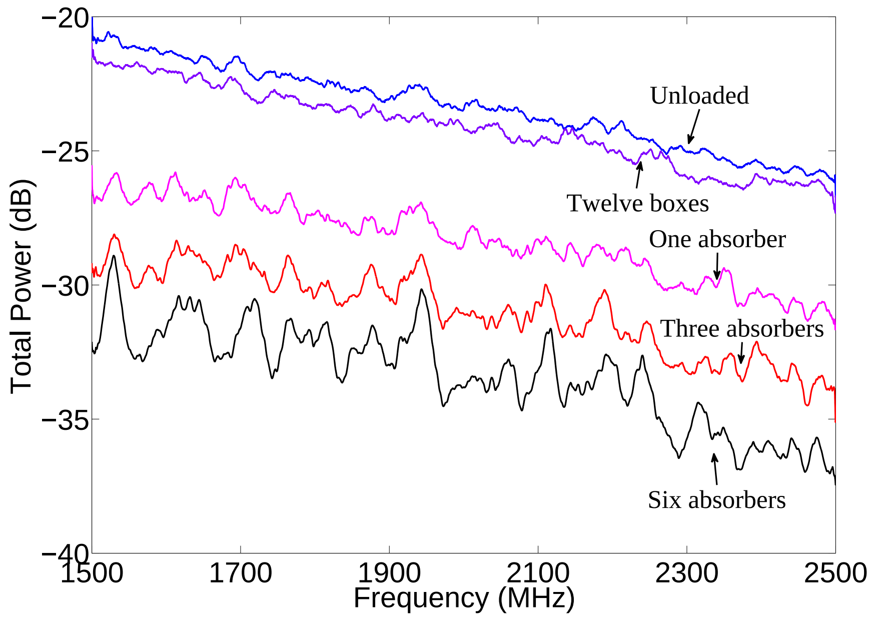

Figure 5.1: Total received power (stirred + unstirred) at monopole 1 as a function of frequency. The data are smoothed over 18.75 MHz by a moving average. The different curves represent different loading configurations.

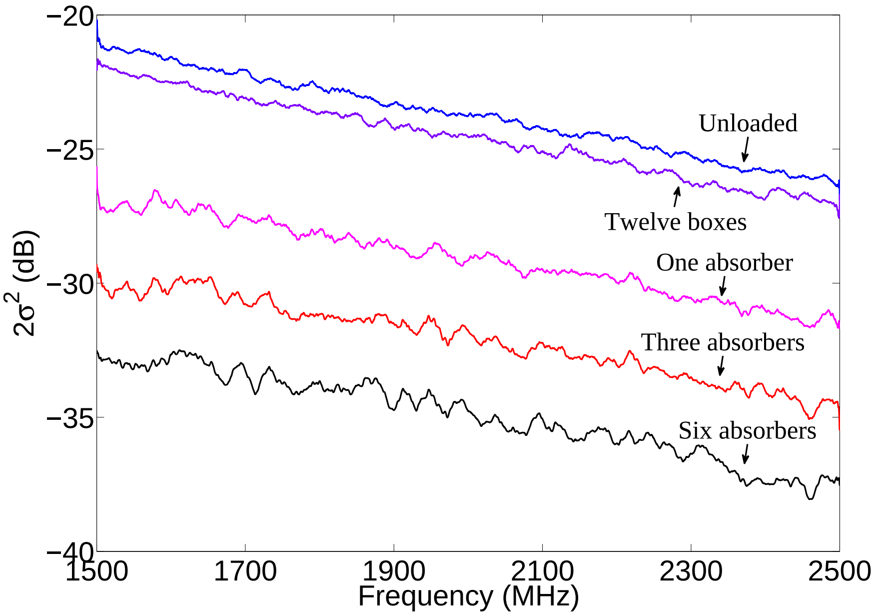

Figure 5.2: Stirred received power at monopole 1 as a function of frequency. The data are smoothed over 18.75 MHz by a moving average. The different curves represent different loading configurations.

reproducibility is a Type A uncertainty. It was determined by calculating the standard deviation from three independent reference measurements. The calculation showed a standard deviation of 0.3 dB for the measurement system reproducibility. The VNA drift is a Type B uncertainty and was determined by measuring the VNA drift over 55 hours. The uncertainty that is associated with the VNA drift is 0.04 dB. The combined uncertainty that comes with our measurements is the root-sum-square of the individual uncertainties. The combined uncertainty is 0.3 dB.

5.2 K-factor

The effect of the loading on the stirred power and the unstirred power is better explained by the K-factor. In Fig. 5.3, the K-factor is plotted for different loading configurations. The K-factor is calculated by averaging the K over the frequency interval 1800 MHz to 2000 MHz. For every monopole (or location) a K is calculated and plotted. To avoid making the graph too crowded, not all loading configurations with the metallic boxes are plotted.

As can be seen, the metallic boxes hardly increase the K-factor. However, the absorbers significantly increase the K-factor. We also see that the K-factor is very different throughout the chamber when loaded with absorbers. The K-factor is especially high at location 3 and location 10, because at those two locations strong unstirred components are received. In Fig. 5.4, we plot the K-factor averaged over 12 locations

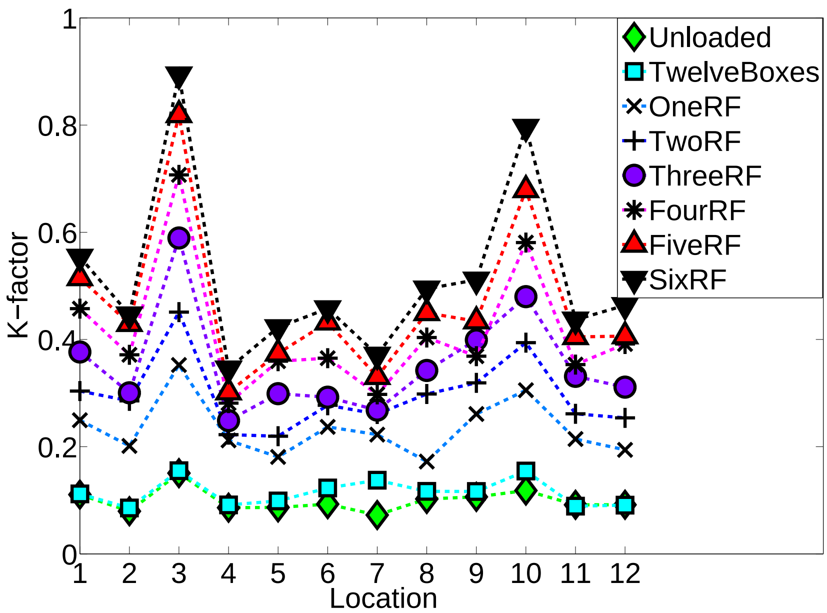

Figure 5.3: K-factor at 12 different locations in the reverberation chamber for various loading configurations. The K-factor at every location is averaged over the frequency interval 1800 - 2000 MHz.

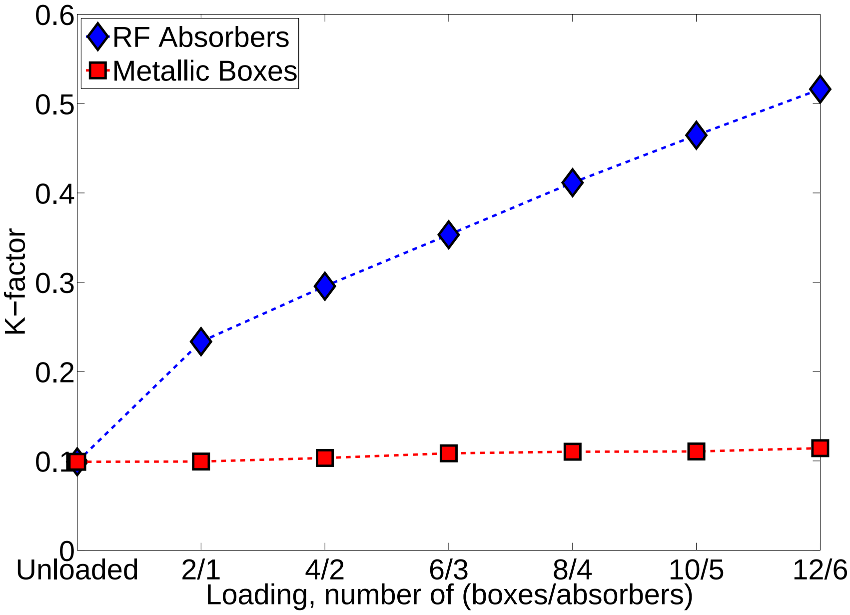

Figure 5.4: K-factor averaged over 12 locations within the chamber as a function of loading. On the x-axis is the number of boxes and the number of absorbers (boxes/absorbers). The line with diamond markers shows the effect of increasing absorbers on the average K-factor. The line with the square markers shows the effect of increasing metallinc boxes on the average K-factor.

for the different loading configurations. It can be seen that the average K is 0.1 for the unloaded chamber, and that it hardly increases with increasing boxes. When the chamber is loaded with absorbers, the average K rapidly increases up to 0.5.

5.3 Coefficient of variation

In Fig. 5.5 six different figures are presented for six different loading configurations. In every figure the total received power of all twelve monopoles are plotted, i.e. twelve curves. It can be seen that the spread between the twelve individual curves increases when the chamber is loaded by absorbers. This spread can be made quantative by calculating C_v by making use of (3.4).

Results for C_v of the total received power are presented in Fig. 5.6. At the 12 positions, 72 samples of the received power were collected. If we assume the samples are independent, the theoretical C_v, calculated from (2.8), results in an C_v of 0.118, or 11.8 %. The coefficient of variation in Fig. 5.6 is averaged over the frequency interval 1800 MHz to 2000 MHz and is expressed in percentage.

The C_v for the metallic boxes is 2 % higher than the theoretical C_v and does not significantly increase with increasing numbers of boxes. The reason why C_v is

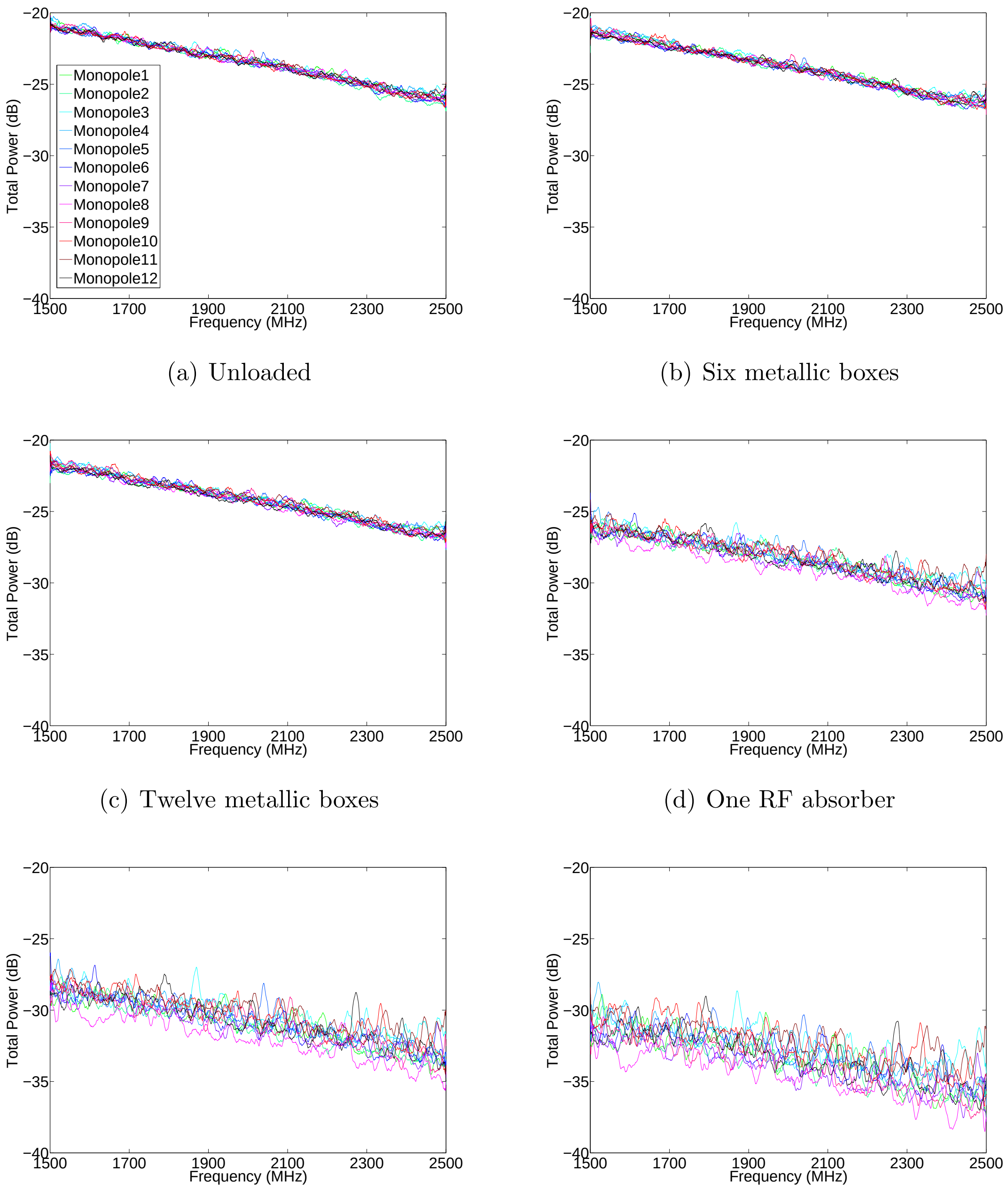

(a) Unloaded

(b) Six metallic boxes

(c) Twelve metallic boxes

(d) One RF absorber

(e) Three RF absorbers

(f) Six RF absorbers

Figure 5.5: Six figures are presented for six different loading configurations. In every figure the total received power of the twelve monopole is plotted as a function of frequency. The spread between the twelve curves increases when the reverberation chamber is loaded with absorbers.

higher than the theoretical is because the field in the chamber is not purely Rayleigh distributed. Unstirred components are present and these components decrease the spatial uniformity. The fact that C_v does not increase with increasing numbers of boxes shows that a large-form-factor device will not degrade the spatial uniformity, as

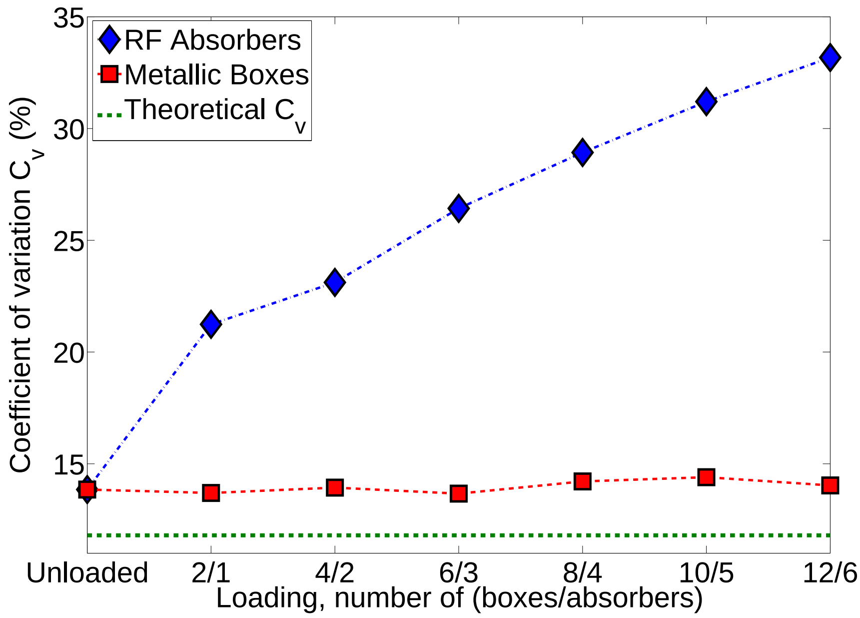

Figure 5.6: Coefficient of variation in percentage of the total received power within the chamber. On the x-axis is the number of boxes and the number of absorbers (boxes/absorbers). The dashed line is the theoretical C_v if the field were purely Rayleigh distributed and 72 independent samples were taken.

long as the surfaces are reflecting.

The C_v with the absorbers increases drastically from 13.6% for the unloaded configuration up to 33.2% for the six RF absorbers configuration. The main cause of this increase is attributed to the drop in Q, see Fig. 4.2. As a result, the stirred energy decreases significantly and the unstirred components become more dominant. This can be seen clearly in Fig. 5.4. The unstirred components are spatially dependent, as can be seen from Fig. 5.3, and will degrade the spatial uniformity.

Next, the C_v was calculated for the received stirred power, and the results are shown in Fig. 5.7. As can be seen, the C_v for the metallic boxes is almost equal to the theoretical value. One possible reason why the measured C_v is slightly higher might be the difference in antenna efficiency between the monopoles. The C_v of the stirred power increases when the chamber is loaded by absorbers. The coefficient of variation increases up to 17.6% for the six RF absorbers configuration. This cannot be due to the unstirred components, since the unstirred components are removed. One reason might be that the 72 samples are not independent anymore, i.e. the samples are correlated. In this case the number of independent samples N_{ind} is lower than 72. A C_v of 17.6% corresponds to approximately 33 uncorrelated samples.

In [21], it is explained that the number of independent samples for one stirrer revolution decreases when the chamber Q decreases. With a lower Q, the paddle is less

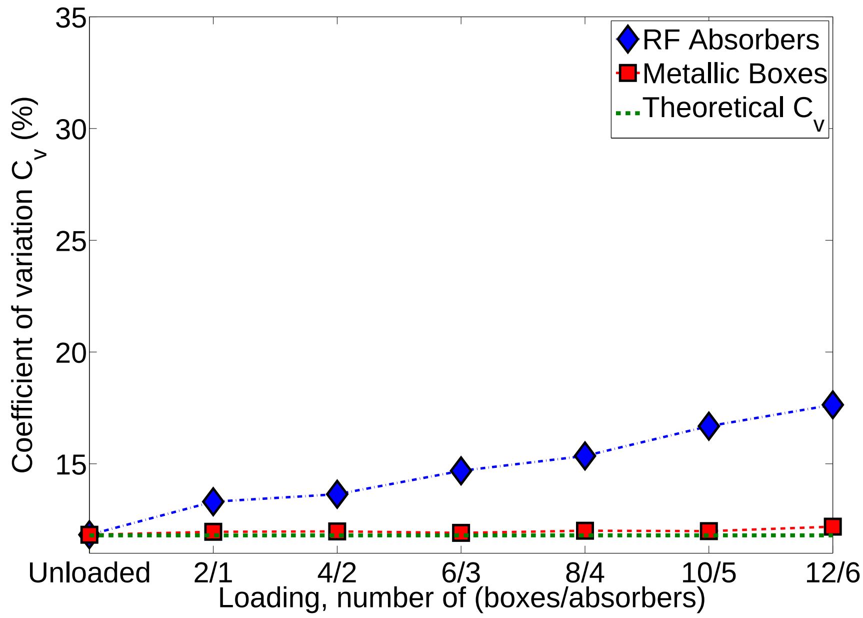

Figure 5.7: Coefficient of variation in percentage of the stirred power within the chamber. On the x-axis is the number of boxes and the number of absorbers (boxes/absorbers). The dashed line is the theoretical C_v if the field were purely Rayleigh distributed and 72 independent samples were taken.

efficient in stirring the EM-fields. In Fig. 5.8, results are presented of the correlation between adjacent samples of the complete data set of 72 paddle positions at 1800 MHz. It can be seen that for increasing absorbers, the correlation between the adjacent samples increases. The samples are considered to be correlated if the correlation exceeds the threshold $^1/_e$. This threshold is commonly applied in reverberation chambers [27]. From Fig. 5.8, we conclude that for more than three absorbers in the reverberation chamber the samples are slightly correlated. This does not completely explain why the C_v increases as much as it does in Fig. 5.7.

In Fig. 5.9 the autocorrelation over the 72 measured samples at 1800 MHz is plotted, for the loading configuration with six absorbers. The presented autocorrelation is an average over all 12 monopoles. Via interpolation between the 5° and the 10° samples, it can be roughly estimated that the samples are uncorrelated at 6°. The number of independent samples can now be calculated from [27]

$$N_{ind} = \frac{360°}{\Delta}. \tag{5.1}$$

In the reverberation chamber Δ can be represented by the stirrer angle offset at which samples are uncorrelated. So with uncorrelated samples at 6° this results in 60 independent samples. This is a rough estimate, but at least it makes clear that there are more independent samples collected than 33 corresponding to 17.6%.

So it can be concluded that there is another reason why the spatial uniformity decreases when absorbers are placed in the reverberation chamber. This reason will be called the proximity effect and will be explained in the next section.

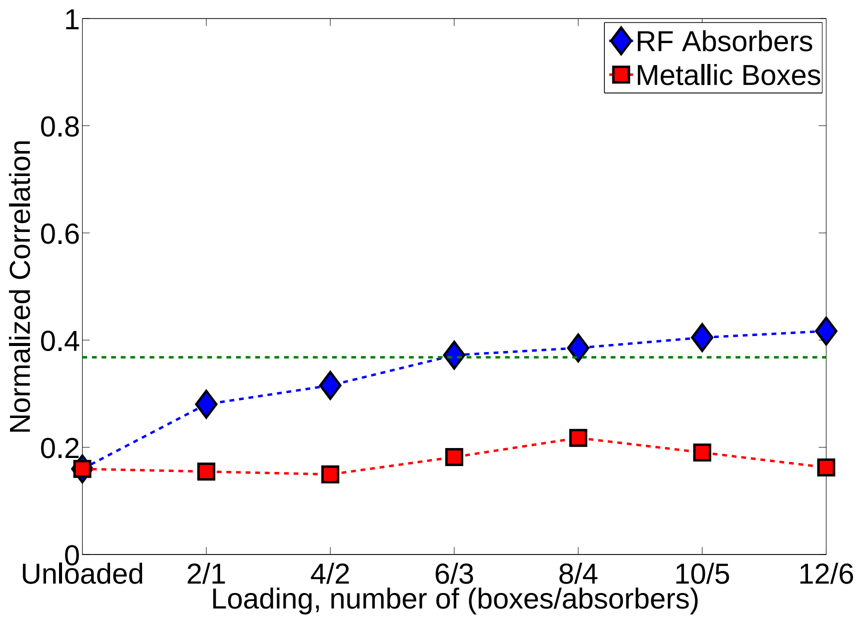

Figure 5.8: Correlation between adjacent samples (5 degree stirrer rotation). On the x-axis is the number of boxes and the number of absorbers (boxes/absorbers). The dashed line is the threshold $^1/_e$

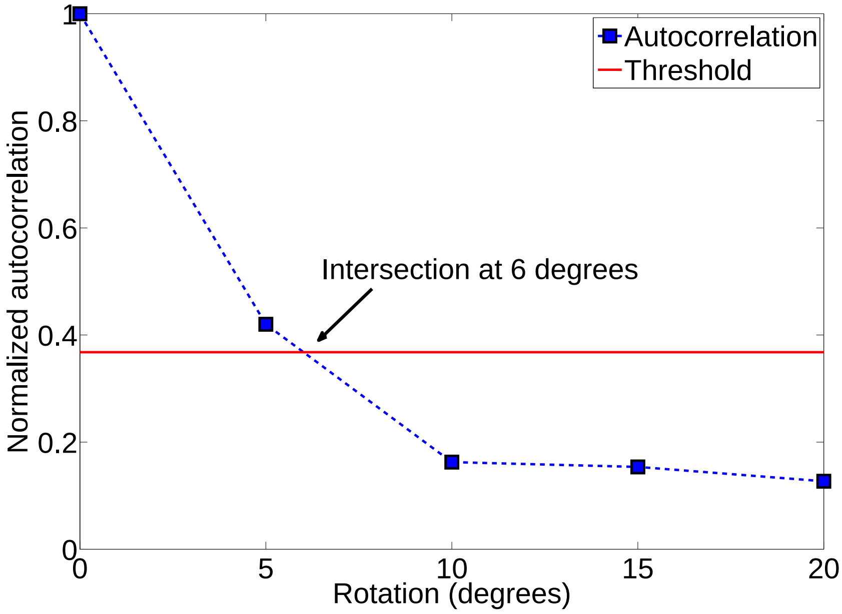

Figure 5.9: The autocorrelation of the measured samples for the loading configuration with six absorbers. Autocorrelation as a function of degree rotation of the stirrer. Intersection with the threshold is indicated. Below this threshold samples are assumed to be independent.

Chapter 6

Proximity Effect

In this chapter the proximity effect is studied. In this first section the definition of the proximity effect will be explained. In the second section experiments and results are presented to validat the proximity effect.

6.1 Definition of the proximity effect

As is explained in [15], the power received by an antenna in the reverberation chamber is independent of the antenna directivity and polarization. The power incident on the antenna has the same mean over every solid angle Ω. Now imagine that an absorber in the chamber occupies some value of steradian Ω_{nr} of a monopole's antenna pattern. This monopole will receive no power from this Ω_{nr}, because an ideal absorber does not reflect EM-waves. Energy that interacts with an ideal absorber is completely absorbed. In this case, the received power is dependent on the orientation of the antenna with respect to the absorber. To make it more obvious, imagine that a directional antenna is pointed directly at an absorber. In this case the antenna will receive much less power than when the antenna is pointed in a direction other than that of the absorber.

The twelve monopoles that were placed throughout the chamber all have a different distance and orientation with respect to the absorbers. Some monopoles could not see the absorbers, because the absorber was in the shadow of their groundplane. Other monopoles were in close proximity and faced towards the absorbers. This resulted in an increase in the standard deviation of received power, which caused a higher C_v Additional experiments were performed to show these effects more clearly.

6.2 Validation of the proximity effect

In Fig. 6.1 the setup is depicted that will be used to show the proximity effects more clearly. A vertically polarized monopole was placed at a horizontal distance of 15 cm from the loading (metallic boxes or RF absorbers). First, the monopole was placed

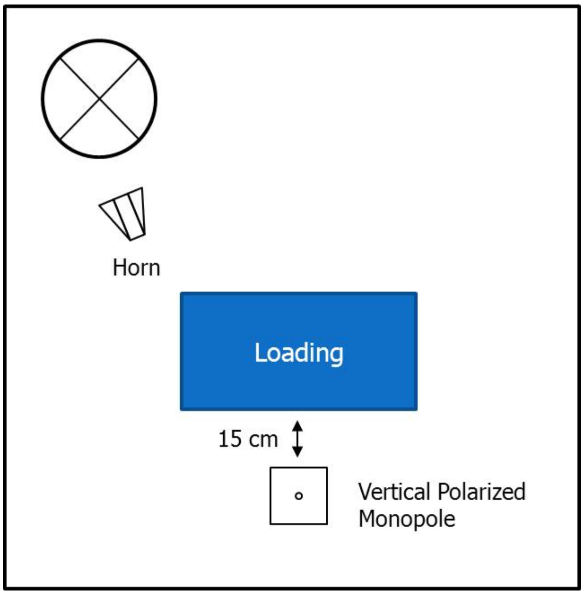

Figure 6.1: View of the setup. A monopole was placed a horizontal distance of 15 cm from the loading.

at a height of 48 cm, referred to as height 1. For every loading configuration, the received stirred power was measured and averaged over the frequency interval 1800 MHz - 2000 MHz. This stirred power was compared to the estimated mean power in the chamber for that particular loading configuration, which was found previously with twelve monopoles. Next, the monopole was placed at a height of 93 cm, referred to as height 2, and the same measurements were repeated.

The results for the metallic boxes are presented in Fig. 6.2. It can be seen that there is no significant difference in received stirred power between height 1 or height 2. The impact of the boxes on the monopole in close proximity is also negligible. The maximum deviation from the estimated mean occurs when the monopole was at height 2 and the chamber was loaded by twelve metallic boxes. For this situation, the monopole received 2.5% less power than the mean. Because the theoretical C_v is 11.8% we conclude that the impact of the boxes on a monopole at 15 cm distance is negligible. This is in agreement with [28] where it was stated that fields approximate their uniform values when the distance from a reflecting boundary is larger than half of a wavelength. At 1.9 GHz, one wavelength corresponds to approximately 15.8 cm.

In Fig. 6.3, results are shown for a monopole in close proximity to absorbers. At height 1 the received stirred power compared to the mean stirred power immediately dropped when an absorber was placed in the chamber. If the monopole was at height 2, the received stirred power relative to the mean stirred power did not drop until three absorbers were stacked. This can be explained by the fact that the monopole at height 2 was higher located than the top of the two stacked absorbers. Since the monopole was vertically polarized on a groundplane, it did not "see" the absorbers.

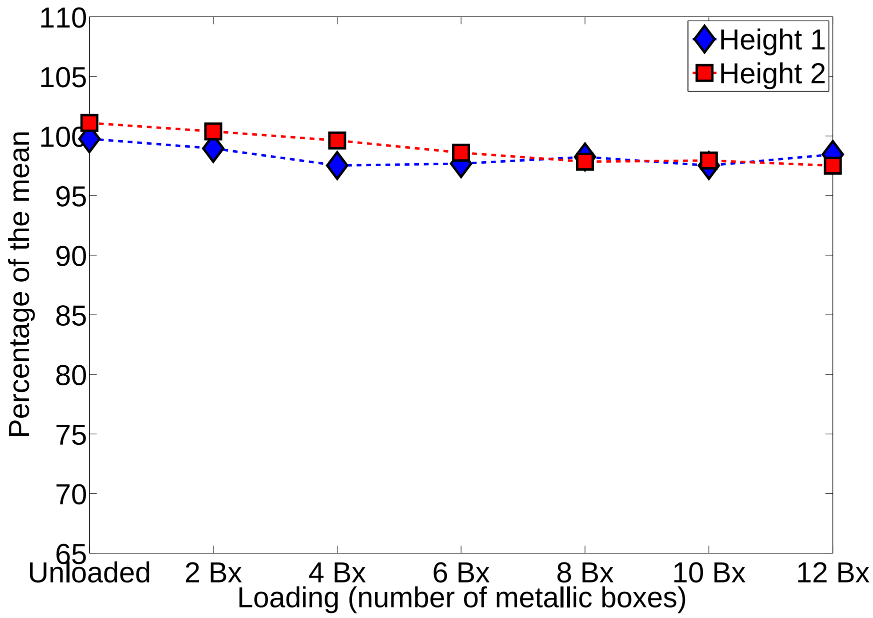

Figure 6.2: The received stirred power for the monopole in close proximity of the metallic boxes. Power is expressed in percentage of the estimated mean stirred power for that particular loading configuration. The power is averaged over the frequency interval 1800 - 2000 MHz. Presented is the received power at height 1 and at height 2.

The monopole at height 2 did not see the absorbers until three absorbers were stacked. At this point, the received stirred power relative to the mean stirred power dropped, because of the proximity effect.

Next, an experiment was performed to show the effect of a decreasing solid angle Ω_{nr}. Two absorbers were stacked in the reverberation chamber, and again a monopole was placed at a 15 cm distance from the absorbers. The monopole was vertically polarized and placed at height 1. The setup was essentially the same as in Fig. 6.1. Again the stirred power was measured and compared to the estimated mean stirred power in the chamber with 2 RF absorbers. The distance between the monopole and the absorber was increased in ten centimeter increments up to 65 cm. For every distance, the received power was measured. By increasing the distance between the monopole and the absorbers, Ω_{nr} decreased. That is, the absorber appeared to be smaller to the monopole. Results are presented in Table 6.1. We see that the impact of the absorber on the received stirred power decreases as the solid angle Ω_{nr} decreases.

The results presented in Fig. 6.3 and Table 6.1 illustrate that the power received by a monopole is dependent on its orientation with respect to an absorber and the distance between the monopole and the absorber. If a monopole is oriented towards an absorber and the absorber is in close proximity of the monopole, it will occupy a large fraction of the antenna pattern. For this reason, the monopole will receive less power. This causes a difference in received power between the monopoles at different locations and with different orientations in the reverberation chamber.

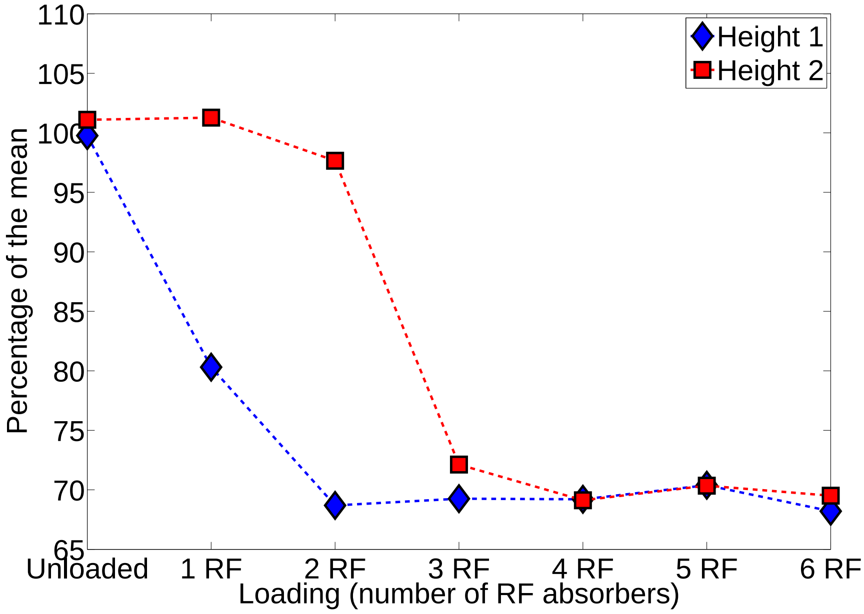

Figure 6.3: The received stirred power for the monopole in close proximity of the RF absorbers. Power is expressed in percentage of the estimated mean stirred power for that particular loading configuration. The powers are averaged over the frequency interval 1800 - 2000 MHz. Presented is the received power at height 1 and at height 2.

Table 6.1: Percentage of the received stirred power compared to the estimated mean power for the 2 RF absorber loading configuration.

Distance (cm)	Percentage of the mean (%)
15	69
25	77
35	85
45	88
55	90
65	94

Chapter 7

Conclusion and Recommendations

In this thesis we investigated the spatial uniformity in a reverberation chamber when loaded by large-form-factor devices. A distinction was made between reflecting and absorbing objects. The chamber was loaded by stacking cardboard boxes wrapped in foil, or by stacking RF absorbers. It was shown that the metallic boxes slightly load the chamber. This loading was caused by the cardboard being lossy. The RF absorbers significantly load the chamber.

The spatial uniformity of the total received power as well as the spatial uniformity of the stirred power were studied. It has been shown that the spatial uniformity of the total power depends on the quality factor. If an absorbing object is put in the chamber, the stirred components decrease, and for this reason the K-factor increases. The unstirred components become more dominant, leading to a degradation of the spatial uniformity with respect to the total received power.

Measurements have shown that a large metallic device does not significantly degrade the spatial uniformity, nor the K-factor. The C_v of the total power was 2% above the theoretical C_v. This is attributed to the fact that the K-factor was not completely zero, whereas the theoretical calculated C_v is based on a pure Rayleigh field distribution. The spatial uniformity of the stirred power if loaded by metallic boxes does agree with the theory.

If absorbers are put in the reverberation chamber, the spatial uniformity of the stirred power does not agree with the theoretical C_v. The reason for this cannot be found from the unstirred components anymore. Rather, the number of independent samples decreases when loading the chamber with absorbers, and that this effect will increase C_v. As discussed, this does not completely explain the increase in C_v. It was shown that another reason for the increase of the C_v is the proximity effect. As explained and experimentally validated, the orientation of an antenna with respect to the absorber affects the received power.

In future work, the effect of absorbers on the spatial uniformity of the stirred power will be further investigated. Of particular interest is what happens to the C_v if it is corrected for the proximity effects and all the samples are independent. If it does not agree with the theoretical C_v, there is an additional phenomenom that degrades the spatial uniformity.

References

[1] C.L. Holloway, D.A. Hill, J.M. Ladbury, P.F. Wilson, G. Koepke, and J. Coder, "On the use of reverberation chambers to simulate a rician radio environment for the testing of wireless devices," *IEEE Trans. Electromagn. Compat.*, vol.54, no.11, Nov. 2006.

[2] E. Genender, C.L. Holloway, K.A. Remley, J. M. Ladbury, G. Koepke, and H. Garbe, "Simulating the multipath channel with a reverberation chamber: application to bit error rate measurements," *IEEE Trans. Electromagn. Compat.*, vol.52, no.4, pp.766-777, Nov. 2010.

[3] D.A. Hill,*Electromagnetic Fields in Cavities.* New York: IEEE Press, 2009.

[4] M.L. Crawford, G.H. Koepke, Design, evaluation, and use of a reverberation chamber for performing electromagnetic susceptibility/vulnerability measurements, NBS Technical Note 1092, April 1986.

[5] D. Zhang, E. Li, "Loading effect of EUT on maximal electric field level in a reverberation chamber for immunity test," *Electromagnetic Compatibility, 2002. EMC 2002. IEEE International Symposium on* , vol.2, no., pp.972-975 vol.2, 19-23 Aug. 2002.

[6] C.L. Holloway, D.A. Hill, J.M. Ladbury, and G. Koepke, "Requirements for an effective reverberation chamber: unloaded or loaded," *IEEE Trans. Electromagn. Compat.* vol.48, no.1, pp.187-194, Feb. 2006.

[7] J.M. Ladbury, P.F. Wilson, G.H. Koepke, and T. Lammers, "Reverberation chamber: An evaluation for possible use as a RF exposure system for animal studies," *Proc. Bio-Electromagnetics Society 25th Annual Meeting*, Maui, HI, Jun. 22-27, 2003.

[8] Electromagnetic compatibility (EMC) Part 4-21: Testing and Measurement Techniques Reverberation Chambers. *IEC Standard 61000-4-21*, 2003.

[9] G.D. Durgin,*Space-Time Wireless Channels.* Upper Saddle River, N.J.: Prentice Hall, 2003.

[10] A.F. Molisch, *Wireless Communications.* New York: Wiley, 2005.

[11] X. Chen, P.-S. Kildal, and S.-H Lai, "Estimation of average rician K-factor and average mode bandwidth in loaded reverberation chamber," *IEEE Antennas Wireless Propag. Lett.*, vol.10, no., pp.1437-1440, 2011.

[12] X. Chen, P.-S. Kildal, C. Orlenius, and J. Carlsson, "Channel sounding of loaded reverberation chamber for over-the-air testing of wireless devices- coherence bandwidth versus average mode bandwidth and delay spread," *IEEE Antennas Wireless Propag. Lett.*, vol.8, no., pp.678-681, 2009.

[13] J.G. Kostas, and B. Boverie, "Statistical model for a mode-stirred chamber," *IEEE Trans. Electromagn. Compat.* , vol.33, no.4, pp.366-370, Nov 1991.

[14] K. Harima,"Statistical characteristics of maximum E-field distribution in a reverberation chamber," *International Symposium on Electromagnetic Compatibility*, vol.2, no., pp. 724- 727 vol.2, 9-13 Aug. 2004.

[15] D.A. Hill, "Plane wave integral representation for fields in reverberation chambers," *IEEE Trans. Electromagn. Compat.* , vol.40, no.3, pp.209-217, Aug 1998

[16] P. Corona, G. Ferrara, and M. Migliaccio, "Reverberating chamber electromagnetic field in presence of an unstirred component," *IEEE Trans. Electromagn. Compat.*, vol.42, no.2, pp.111-115, May 2000.

[17] J. Page, "Stirred mode reverberation chambers for EMC emission measurements and radio type approvals or organised chaos," *Ninth International Conference on Electromagnetic Compatibility*, pp.313-320, 5-7 Sep 1994

[18] D.A. Hill, J.W. Adams, M.T. Ma, A.R. Ondrejka, B.F. Riddle, M.L. Crawford, and R.T. Johnk, "Aperture excitation of electrically large lossy cavities," Nat. Inst. of Standards, Boulder, CO, 1993, *NIST Tech. Note 1361.*

[19] A. Papoulis, *Probability, Random Variables and Stochastic Processes.* New York: McGraw-Hill, 1984, pp 249.

[20] P.-S. Kildal, C. Carlsson, and J. Yang, "Measurement of free-space impedances of small antennas in reverberation chambers." *Microw. Opt. Technol. Lett.*, vol. 32, pp. 112-115, 2002.

[21] P. Hallbjörner, "A model for the number of independent samples in reverberation chambers," *Microwave Opt. Technol. Lett.*, vol. 33, no. 1, pp. 25-28, Apr. 2002.